Microstructural and magnetic characterization of nanostructured α-Fe_2O_3 and CuO mixtures obtained by ball milling

2001 J. Phys.: Condens. Matter 13 1743

(http://iopscience.iop.org/0953-8984/13/8/311)

INSTITUTE OF PHYSICS PUBLISHING JOURNAL OF PHYSICS: CONDENSED MATTER

J. Phys.: Condens. Matter **13** (2001) 1743–1757 www.iop.org/Journals/cm PII: S0953-8984(01)16782-2

Microstructural and magnetic characterization of nanostructured α-Fe_2O_3 and CuO mixtures obtained by ball milling

S J Stewart[1,5], R A Borzi[2], G Punte[2], R C Mercader[2] and F Garcia[3,4]

[1] Department of Chemistry, The Open University, Walton Hall, Milton Keynes MK7 6AA, UK
[2] Departamento de Física, Universidad Nacional de La Plata, CC 67, 1900 La Plata, Argentina
[3] Centro Brasileiro de Pesquisas Físicas (CNPq), Rua X Sigaud 150, 22290-180 Río de Janeiro, Brazil
[4] Laboratório Nacional de Luz Síncrotron, CxP 6192, CEP 13083-970, Campinas SP, Brazil

E-mail: stewart@venus.fisica.unlp.edu.ar

Received 1 September 2000, in final form 15 November 2000

Abstract

We have subjected powder mixtures of $(0.5x)\alpha$-Fe_2O_3 and $(1-x)$CuO to ball milling for a fixed period of 10 h for several x across the whole range of concentrations. No phases other than the initial ones in their nanostructural form were detected within the resolution of the several experimental techniques employed. The grain size of the CuO nanoparticles is not observed to depend notably upon x and the microstrain is three times higher than that found for haematite. In contrast, the α-Fe_2O_3 grain size varies with the haematite content of the mixtures and a minimum size of $D \approx 70$ Å was observed for $0.50 \leqslant x \leqslant 0.95$. The high-field susceptibility can be expressed as the weighted sum of the milled CuO and α-Fe_2O_3 individual susceptibilities. For low x, a Cu(Fe)O solid solution is formed. An increase in the overall magnetization is observed for intermediate concentrations. In addition, within this x range, a broad Mössbauer sextet related to grain boundary regions is found coexisting with a bulk α-Fe_2O_3 signal at 30 K. The relative area of this broad signal is a maximum for $x = 0.67$, a sample that also shows an anomalous magnetic hysteresis. We associate these facts to a state of spin disorder linked to the grain boundaries of the nanocrystalline material.

1. Introduction

Ball milling (BM) has been employed to obtain supersaturated alloys, metastable phases and amorphous materials, and to prepare nanostructured materials [1]. When mixtures of two or more materials are mechanically milled an alloying or a mechano-chemical reaction can take place if the mixture is composed of metals or non-metals, respectively. In metal–ceramic

[5] Corresponding author. Permanent address: Departamento de Física, UNLP, CC 67, 1900 La Plata, Argentina.

systems, a displacement reaction can occur and materials with enhanced magnetic properties are obtained [2]. Previous results on mixtures of Fe and Cu metals indicate that BM drastically increases the solubility range, and the final phase achieved depends on the atomic concentration of the constituents [3]. When mixtures of non-metallic systems are ball milled, a reduction of the particle size to a nanoscale occurs, before a reaction can take place [4]. BM, by its nature, forces the particles to be in close contact, and thus, in magnetic materials, interparticle interactions become evident. In this case, the competition between the magnetic anisotropy and crystallinity obscures the conclusions that can be drawn as to what parameters are relevant in the final magnetic state. In addition, open issues are involved in an accurate characterisation of ball-milled materials. For instance, surface layers with features characteristic of spin-glass-like systems have been identified in both metallic [5] and oxide [6] milled compounds. The spin disorder at the particle surface manifests as an enhancement of the high-field magnetization in antiferromagnets [7, 8], in the occurrence of irreversibility at high fields in ferrimagnets [6] or leads to peculiar hysteresis effects [6, 8]. Mössbauer studies performed on iron-containing ball-milled systems showed that the distorted environment sensed by the Fe nuclei located at the grain boundaries gives rise to a signal that differs from that of the bulk material [9].

Haematite (α-Fe_2O_3) and tenorite (CuO) are both antiferromagnetic materials with Néel temperatures (T_N) of 950 and 230 K respectively, and each presents a peculiar magnetic behaviour. On the one hand, α-Fe_2O_3 undergoes a transition from a weakly ferromagnetic (WF) state to an antiferromagnetic (AF) one at the Morin temperature, $T_M = 263$ K [10]. On the other, CuO presents low-dimensional features, with a transition from a paramagnetic to an incommensurate phase at 230 K and a second transition to a commensurate one at 213 K [11]. Under certain conditions, when α-Fe_2O_3 is subjected to prolonged BM, a phase transformation to Fe_3O_4 occurs [12]. Recently, we have reported that strongly interacting weak ferromagnetic α-Fe_2O_3 nanoparticles can be obtained by BM of pure haematite in air [13]. In the case of CuO, the effect of the reduced grain size and defects induced by the milling is to increase the susceptibility, which has a Curie–Weiss behaviour above T_N [14]. As far as ball milling of α-Fe_2O_3/CuO mixtures is concerned, a metastable solid solution Cu(Fe)O has been obtained in the low-haematite-content region [15]. On the other hand, the spinel $CuFe_2O_4$ has been reported to be formed after a high-energy milling of a mixture in a 1:1 molar ratio for 17 days [16].

In this work, through ball milling of CuO and α-Fe_2O_3 mixtures, nominal solid solutions $Cu_{1-x}Fe_xO_{1+1/2x}$ have been prepared over the range of concentrations $0 \leqslant x \leqslant 1$ to add to the better understanding of the character of the phases in this ball-milled ceramic system. Using x-ray diffraction, transmission electron microscopy, Mössbauer spectroscopy and magnetization measurements, the magnetic behaviour of the ensuing phases is analysed in connection with the structural parameters, grain size and interparticle interactions.

2. Experiment

Mixtures of CuO (Cerac, 99.999% purity, 20 mesh) and α-Fe_2O_3 (Cerac, 99.99% purity, 325 mesh), with a relation $(1-x)$CuO+$(x/2)Fe_2O_3$, were used as starting materials to prepare solid solutions of nominal composition $Cu_{1-x}Fe_xO_{1+1/2x}$ ($x = 0.03$, 0.10, 0.30, 0.50, 0.67, 0.80, 0.95). These mixtures, as well as pure CuO and α-Fe_2O_3 (i.e. $x = 0.00$ and 1.00, respectively), were mechanically ground for 10 h. The milling was carried out in air in a cylindrical steel vial with one steel ball using a vertical vibratory mixer mill operating at $\approx$50 Hz. The ball-to-powder mass ratio was 20:1. The total amount of sample used during each milling was 100 mg. The x-ray diffraction (XRD) characterisation was carried out in a Philips PW-1710 diffractometer. Cu Kα ($\lambda = 1.5406$ Å) radiation was used to obtain data in

the $15 \leqslant 2\theta \leqslant 110^\circ$ range, with steps of 0.02° and counting time not less than 15 s per step. A Rietveld analysis was performed on all the obtained patterns using the program DBWS-9411 [17]. The line breadths of the selected experimental peaks of each phase were obtained with WINFIT [18].

Transmission electron microscopy (TEM) analyses were performed in a JEOL JEM-2000FX microscope operating at 200 keV. All samples were subjected to energy dispersive x-ray analyses (EDX).

The Mössbauer spectra at room temperature (RT) and at 30 K (LT) were taken in transmission geometry with a nominal 50 mCi ^{57}Co source in a Rh matrix. Isomer shifts (δ) are referenced to α-Fe at room temperature (RT). The absorbers were prepared with $\approx$18 mg cm^{-2} of sample required for optimum thickness. To improve the Mössbauer absorption, enriched $^{57}Fe_2O_3$ was employed in samples with concentrations $x = 0.03$ and 0.10. The spectra were fitted with a non-linear least-squares program to Lorentzian line-shapes with constraints.

Magnetization (M) measurements at RT and at 10 K were taken over selected samples ($x = 0.00$, 0.67, 0.80, 0.95 and 1.00) using a commercial SQUID magnetometer, in fields (H) up to 50 kOe.

3. Results

3.1. XRD and TEM characterization

The XRD patterns of the ball-milled samples are shown in figure 1. Patterns belonging to well crystalline samples of the starting materials, CuO and α-Fe_2O_3, are also included for comparison. The overlapping of the CuO and α-Fe_2O_3 characteristic lines and the considerable broadening resulting from the milling process make it difficult to identify the contribution of each oxide in the whole range of concentrations. In spite of the complexity of the patterns and the fact that it was not possible to disregard the possibility that traces of other phases could be contributing to them, the two-phase model proposed in the Rietveld analysis renders relatively goods fits.

Using the Scherrer equation ($K = 1$), we estimated for CuO and α-Fe_2O_3 the volume-average crystallite dimension [19], D_S, as a function of x. The haematite D_S (figure 2) was calculated using the breadth of the (104) reflection line. For $x = 0.03$ the large error associated with the low haematite content and the already mentioned overlap and broadening of the lines prevent a reliable determination. The tenorite D_S was calculated from the breadth of the $(11\bar{1})$ line. In this case, due to the strong broadening of the CuO lines, the estimation could only be done for samples with $x < 0.80$. CuO average size was found to be almost unaffected by the presence of haematite. It remains constant, within errors, with varying concentration, centred on $D_S = 45 \pm 10$ Å.

Considering the sample preparation process, microstrain cannot be neglected as a source of broadening of the Bragg peaks. From the Rietveld refinement results and by application of the Delhez *et al* [20] method to the same peaks that were analysed previously, we were able to discriminate the average volume-weighted crystallite size, D_D, and the weighted average strain, $\tilde{\varepsilon}$, contributions. The similarity of the D_S and D_D dependences on x for haematite (figure 2) would indicate that the presence of CuO does not enhance considerably the strain induced by the BM. On average, CuO D_D remains constant with x ($D_D = 75 \pm 20$ Å). It is seen that the difference between D_S and D_D is larger for CuO than for haematite, reflecting the higher strain in tenorite particles. In fact, the $\tilde{\varepsilon} = 0.013 \pm 0.002$ value estimated for CuO is three times that found for α-Fe_2O_3. Regarding the α-Fe_2O_3 grain size (figure 2), the results show that the grinding process reduces by an order of magnitude the size of the

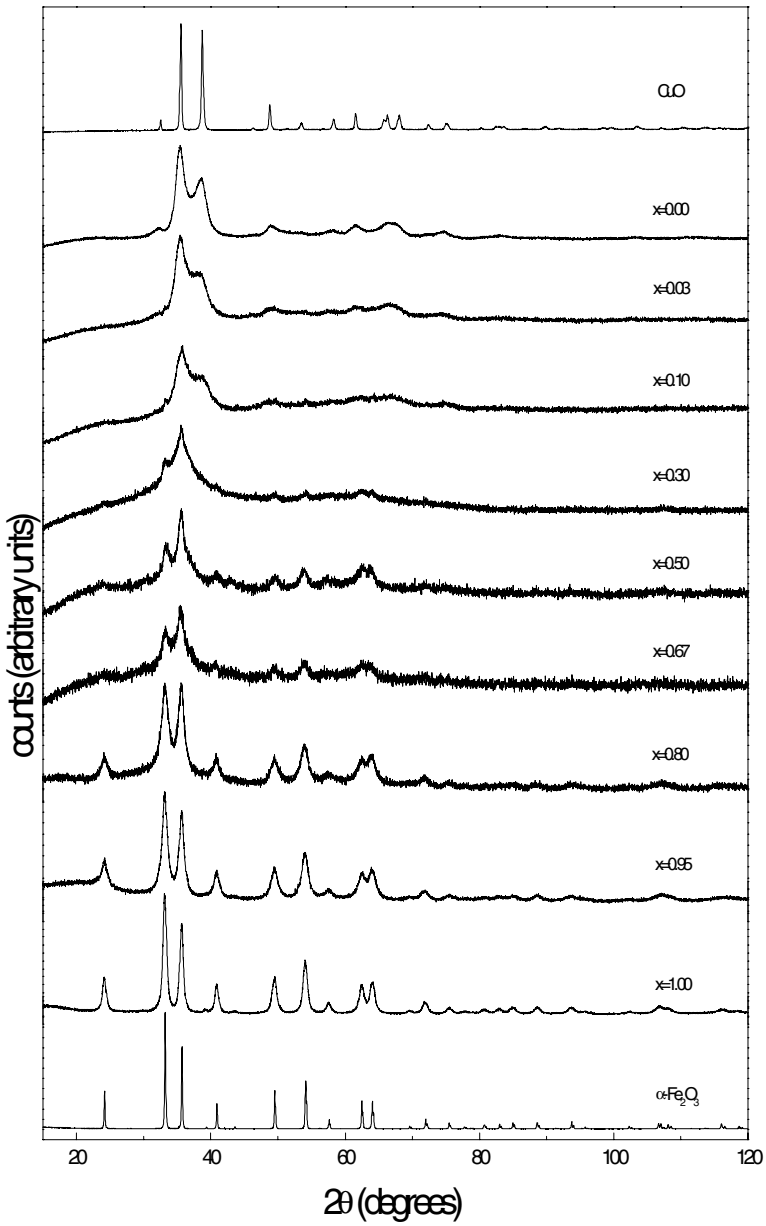

Figure 1. X-ray diffraction patterns of the ball-milled samples. Patterns of the starting materials, CuO and α-Fe_2O_3, are also included.

$x = 1.00$ sample with respect to the initial material. Moreover, it leads to a final size that depends significantly on the composition. Indeed, further decrease is induced by the presence of CuO in the haematite-rich region. In samples with $x < 0.50$ an increase in haematite D_D is observed. It is worth noting that the BM process produces smaller crystallites for CuO (i.e. $x = 0.00$, 73 ± 12 Å) than for α-Fe_2O_3 ($x = 1.00$, 140 ± 12 Å), in accordance with the hardness of CuO and α-Fe_2O_3 [21].

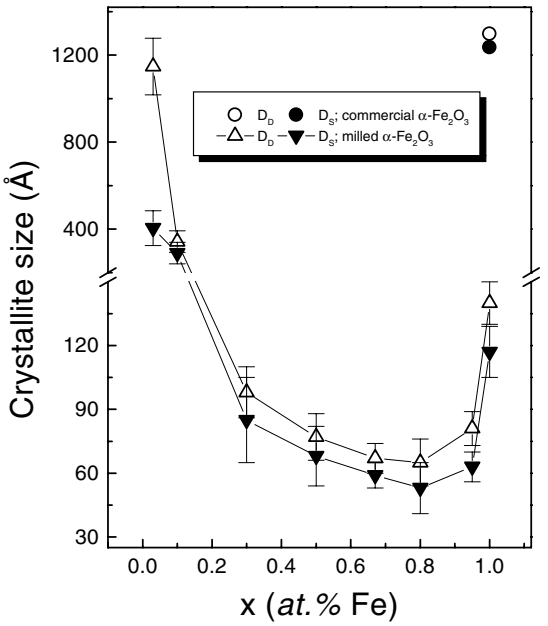

Figure 2. Crystallite dimensions of α-Fe_2O_3 (D) versus the iron content x, determined using the Scherrer equation (D_S) and the Delhez method (D_D).

TEM micrographs showed that the ball-milled powders are in a high state of agglomeration, with particle sizes at least one order of magnitude larger than those estimated by the XRD analyses. Small units of $\approx$14 nm can be distinguished at the edges of the highly agglomerated haematite powder for the $x = 1.00$ sample. This particle size is close to the crystallite size that results from the XRD data analysis. No impurity elements were detected by EDX analyses.

3.2. Mössbauer results

The Mössbauer spectra are shown in figure 3. Up to $x = 0.80$ the RT spectra show the co-existence of a broad doublet and a sextet. The resolved sextet belongs to α-Fe_2O_3. In all cases, the central non-magnetic signal has an Fe^{3+} isomer shift and the quadrupole splitting, Δ, is within the 0.9–1.3 mm s^{-1} range. Although the doublet might be present in the RT spectra of $x = 0.95$ and $x = 1.00$ samples, the particle size distribution and the relaxation behaviour displayed in these cases broaden considerably the lines and do not allow the identification of their individual contributions. However, since we are mainly interested in their relative areas and not in the relaxation or hyperfine field distribution details, we have simulated their combined effect by including a broad single line in the fit. The same procedure was performed on other spectra where relaxation features appeared. In addition, other magnetic components with broad line-widths were included in the fitting when needed. At RT, the contribution to the overall Mössbauer spectra due to the sextet attributed to α-Fe_2O_3, decreases as x increases up to $x = 0.50$, and increases for $x \geqslant 0.67$ (figure 4(a)).

Except for $x = 0.10$, the spectra for all concentrations experience major changes when the temperature is lowered (figure 3). Due to their complexity, we start to analyse them in terms of the sub-spectra that belong to the well resolved α-Fe_2O_3 signal. The spin-flip that occurs at the Morin transition in bulk pure haematite is clearly detected using Mössbauer

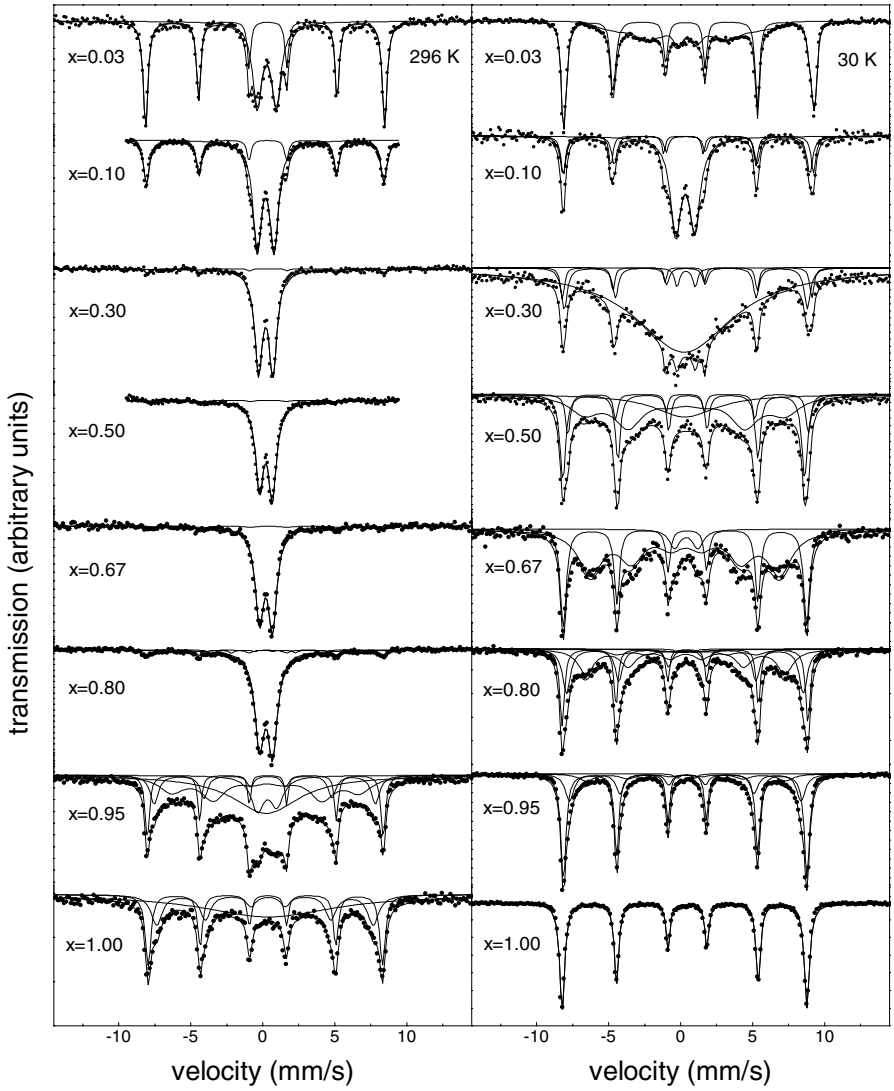

Figure 3. Mössbauer spectra of the ball-milled samples taken at room temperature (left) and at 30 K (LT) (right).

spectroscopy [10]. Indeed, the quadrupole shift (2ε) changes from -0.20 to 0.40 mm s^{-1} as the magnetic phase goes from the WF state to the AF one. When the oxide is composed of fine particles, presents defects or isomorphous substitution incorporates water or OH groups, the region of temperature where the transition takes place broadens considerably and T_M decreases, and furthermore the transition can be suppressed [22]. In our case, the LT α-Fe_2O_3 sextet (hyperfine field $B_{hf} > 50$ T) has been fitted considering two components to account for the two possible magnetic states (figure 3). Table 1 shows that the average 2ε values at 30 K are positive for low x, gradually becoming negative for increasing iron concentration indicating that the transition is gradually suppressed as x increases. Furthermore, the $2\varepsilon \approx -0.20$ mm s^{-1} value at LT registered for the ball-milled pure α-Fe_2O_3 ($x = 1.00$) shows that the oxide remains

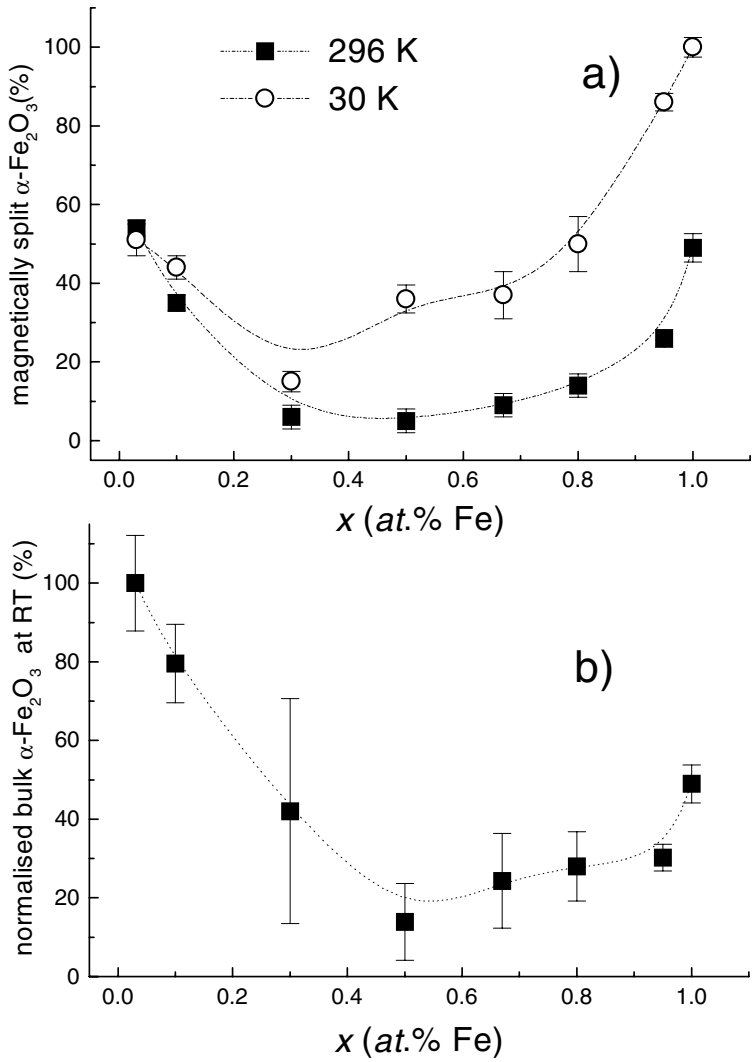

Figure 4. (a) Relative area of the Mössbauer signal that belongs to magnetically split α-Fe_2O_3 at room temperature (RT) and 30 K. (b) Relative area of resolved α-Fe_2O_3 at RT (normalized to the relative area of resolved α-Fe_2O_3 at 30 K) as a function of x. The dashed lines are guides for the eye.

in its WF phase down to 17 K [13]. We take the superparamagnetic (SPM) α-Fe_2O_3 fraction at RT (within the Mössbauer characteristic time $\tau_{mos} \approx 10^{-8}$ s) as the difference between the well resolved haematite fraction at LT and RT. It can be seen that this SPM fraction is negligible at low x and increases almost linearly with x (figure 4(a)). In addition, as x increases, the line-width broadens and the B_{hf} values decrease with respect to the 53.8 T recorded for $x = 0.03$ (table 1). These facts are clear evidence that, in accordance with the XRD results, at low x the α-Fe_2O_3 crystallinity is relatively less affected by the milling.

The RT spectrum for $x = 1.00$ comprises the contribution of low B_{hf} and does not show the co-existence of a sextet and a doublet that is typical of systems of non-interacting small particles with a size distribution. Except for this sample, which clearly shows only one site

Table 1. Hyperfine parameters obtained from the Mössbauer spectra taken at 30 K by the fitting procedure described in the text. x indicates the iron content, B_{hf} hyperfine field, Δ quadrupole splitting, δ isomer shift, 2ε quadrupole shift, Γ linewidth and I relative area of the signal. Errors are quoted as subscripts.

x	B_{hf} (T)	Δ (mm/s)	δ (mm/s)	2ε (mm/s)	Γ (mm/s)	I (%)
0.03	53.8_5		0.48_1	0.26_1	0.31_1	51_4
	30.1_5		0.52_4	0.03_7	1.5_1	32_6
			0.37_{10}		4_1	17_4
0.10	53.9_5		0.47_1	0.34_2	0.25	19_2
	53.2_5		0.48_1	0.05_2	0.36_2	24_2
		1.32_2	0.43_1		0.90_2	57_3
0.30	53.8_5		0.48_1	0.14_3	0.25_3	5_2
	52.4_5		0.47_1	-0.00_3	0.40_5	10_2
		1.26_6	0.48_3		0.41_1	2_1
			0.35		8.1	83_3
0.50	51.9_5		0.52_1	0.20_3	0.27_5	10_2
	52.1_5		0.46_1	-0.29_2	0.36_3	26_3
	43_1		0.45_5	-0.11_7	2.3_2	44_6
			0.4_1		5.2_9	20_4
0.67	52.7_5		0.49_1	-0.16_2	0.27_2	24_3
	50.0_5		0.48_2	-0.20_4	0.5_1	13_3
	40.0_5		0.43_3	-0.08_5	1.7_1	57_5
		1.5_1	0.49_5		0.9_1	6_1
0.80	53.1_5		0.48_1	-0.15_1	0.25_2	23_3
	51.3_5		0.48_1	-0.17_1	0.47_4	27_4
	43.5_5		0.45_2	-0.04_4	1.7_1	47_4
		1.92_8	0.49_3		0.7_1	3_1
0.95	52.5_5		0.48_1	-0.14_1	0.30_1	60_2
	50.0_5		0.48_1	-0.12_1	0.57_1	26_1
	43_1		0.47_6	0.02_9	1.8_1	12_2
		1.2_1	0.48_1		0.50_4	2_1
1.00	52.8_5		0.48_1	-0.20_1	0.31_1	100

that corresponds to α-Fe_2O_3 in its WF state, the spectra display other components at LT. These signals cannot be assigned straightforwardly to any phase or phases. In addition, the magnetic behaviour is diverse as x increases, suggesting that these signals might have different origins depending on the x range. In an attempt to clarify the possible origins of these signals, we distinguished two behaviours at 30 K.

(i) For the $x = 0.03$ sample the doublet observed at RT has almost disappeared giving rise to a sextet with very broad lines and a $B_{hf} \approx 30$ T (figure 3). This signal resembles the one assigned to a low-iron-containing Cu(Fe)O solid solution [15, 23, 24]. For $x = 0.10$, we found that the doublet and the sextet almost preserve their relative populations as the temperature is lowered (table 1). This indicates that the unsplit signal that originates the doublet at RT does not order magnetically or block within the temperature range measured.

(ii) The complex LT sub-spectrum of $x = 0.30$ involves a component with a relatively low B_{hf} (table 1). As x increases, this component evolves towards a more resolved site with a higher B_{hf} value ($\approx$43 T). This signal is present within a concentration range where α-Fe_2O_3 has achieved a minimum grain size (see figure 2). For $x \geqslant 0.80$, the population of the broad magnetic signal gradually decreases—while the average α-Fe_2O_3 grain size

slightly increases—and finally disappears in the 30 K spectrum of the ball-milled pure α-Fe_2O_3.

3.3. Magnetization measurements

The M–H curves taken at both RT and 10 K are shown in figure 5. These curves do not reach a saturation value up to the maximum applied field (50 kOe). They follow the linear behaviour typical of AF systems for $H \geqslant 20$ kOe, excepting $x = 0.67$ at 10 K, that shows hysteresis up to ≈30 kOe. For samples $x = 0.67$ and 0.80, M increases more rapidly at low fields and reaches higher values at high fields, in comparison with M of samples $x = 0.00$, 0.95 and 1.00. In particular, the $x = 0.67$ sample exhibits the highest M values and shows an anomalous $M(H)$ behaviour at 10 K, with an initial magnetization curve that lies below the remagnetizing one. These facts might suggest that some kind of spin disorder is achieved at LT in the $x = 0.67$ sample [8]. The extrapolation to $H = 0$ of the linear dependence at high fields yields the residual magnetization M_0, while the high-field susceptibility χ_H is obtained by its slope (figure 6). The low values of M_0 are a further indication that the milled mixtures are mainly composed of fine particles of the initial copper and iron oxides. If copper ferrite or magnetite had been formed during the milling process, it must only have been in very small amounts. Indeed, both are ferrimagnetic materials whose magnetization, in bulk [25] or BM samples [16], is an order of magnitude higher than that measured in our case. Besides, χ_H at 10 K can be expressed approximately by the linear relation $(1 - x)\chi_0 + x\chi_1$, where χ_0 and χ_1 are the χ_H of milled CuO and α-Fe_2O_3 samples, respectively (figure 6). The coercitivity H_c is almost negligible at RT for $x = 0.00$, 0.67 and 0.80 (table 2), denoting an SPM state, sensed within the temporal window that characterizes these experiments (≈100 s). A relatively higher H_c value is observed for $x = 0.95$ and 1.00 at both 10 and 300 K. At 10 K, the increment observed in H_c evidences the blocking of the magnetic moments of the particles.

Table 2. Coercive forces (H_c) obtained from the M–H curves, at room temperature and 10 K.

	$x = 0.00$	$x = 0.67$	$x = 0.80$	$x = 0.95$	$x = 1.00$
H_c at 300 K (kOe)	0.08	0.08	0.07	0.27	0.27
H_c at 10 K (kOe)	0.23	0.18	0.28	0.75	0.75

4. Discussion

4.1. Dependence of the α-Fe_2O_3 grain size with the composition of the mixtures

The analyses of the x-ray patterns show that after BM α-Fe_2O_3 and CuO mixtures, nanosized particles were obtained for all x values. The Rietveld analysis and the magnetization results indicate that the spinel $CuFe_2O_4$ (or $Cu_xFe_{3-x}O_4$) was not formed in appreciable amounts. In contrast, the Mössbauer results show the presence of other signals different from α-Fe_2O_3 in a blocked or SPM state. The possible source of these Mössbauer signals will be further discussed in section 4.3.

The non-monotonic behaviour of the α-Fe_2O_3 crystallite sizes that results from the XRD analysis is also reflected in the Mössbauer measurements. Indeed, the normalized fraction of well resolved α-Fe_2O_3 at RT as a function of x (figure 4(b)) presents similar features to that of D_S and D_D (figure 2). However, strong interactions between single domains [13] might influence a precise determination of the α-Fe_2O_3 fraction for high x values.

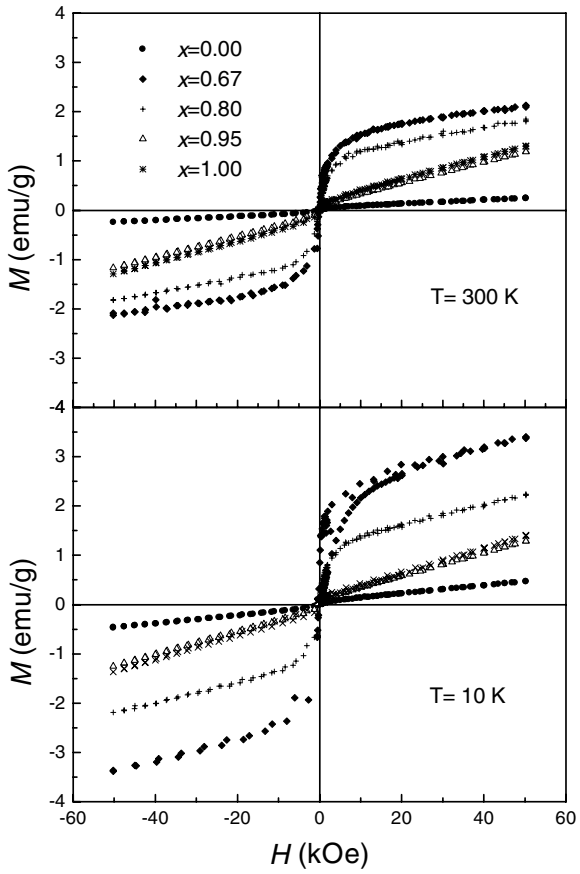

Figure 5. Magnetization (M) curves up to an applied magnetic field (H) of 50 kOe taken at room temperature and at 10 K.

The fact that α-Fe_2O_3 shows almost bulk features for low x agrees with the relative hardness of the oxides involved. Indeed, the hardness of tenorite is between 3.5 and 4 on the Mohs scale for minerals, while a value between 5 and 6 was reported for haematite [21]. This implies that haematite would resist scratching by tenorite. Thus, for low x, the softer material, i.e. CuO, mainly absorbs the energy delivered during the mechanical process. Since haematite would scratch itself, when x increases so would the chance that the α-Fe_2O_3 particles absorb an important fraction of the energy transferred during milling. Ball milling of a CuO/Cr_2O_3 mixture also showed that CuO was more affected by the stresses applied during the milling than the harder Cr_2O_3 [26]. At the high-x end, the α-Fe_2O_3 crystallite size increases (figure 2). The difference between $x = 0.95$ and $x = 1.00$ indicates that the presence of even small quantities of CuO influences the milling process. Furthermore, other parameters distinct from the mechanical ones—e.g. Cu diffusion into the α-Fe_2O_3 matrix—may also play a role in the final microstructure.

4.2. Low-x region: $Cu_{1-x}Fe_xO$ solid solution

The hyperfine parameters of the non-magnetic component observed at RT are in good agreement with many high-spin Fe^{3+} doublets originated in SPM iron oxides [27, 28].

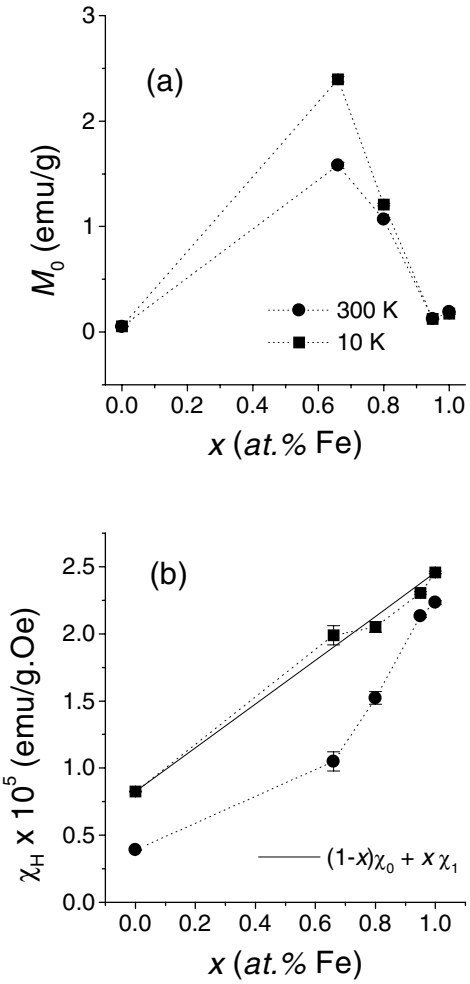

Figure 6. Residual magnetization M_0 obtained after the extrapolation to $H = 0$ of the linear behaviour at high fields (a), and its slope that accounts for the high-field susceptibility χ_H (b). The dashed lines are a guide for the eye.

Indeed, these systems are characterized by a poorly crystalline state and a distribution of particle sizes that gives rise to the broad line-widths of the Mössbauer signals.

For the $x = 0.03$ sample, as the temperature is lowered, the doublet becomes a broad magnetic signal which displays similar features to that associated with a Cu(Fe)O solid solution, where the Fe probe is sensing the complex magnetic behaviour of CuO [15]. This solid solution is known to exist in the Cu–Fe–O system—for low iron concentrations—both for the ball-milled sample [15] and that prepared by co-precipitation [23, 24].

In the $x = 0.10$ case, the relative population of α-Fe_2O_3 shows a slight increase at LT, evidencing that some SPM particles contribute to the doublet at RT. The fact that more than half of the total Fe signal corresponds to a non-magnetic component might indicate that if the Cu(Fe)O solid solution was formed, the concentration of Fe ions within the CuO structure ($\approx$5 at.%) is higher than in the 0.03 sample. These impurities might interrupt the Cu^{2+}–O^{2-}–Cu^{2+} superexchange paths that lead to the long-range magnetic ordering in CuO,

and thus produce a lowering of T_N. A similar result was found by Masterov *et al* [23], in a Cu(Fe)O solid solution. In this work, doping with Fe^{3+} diminished the resolution of the hyperfine structure with increasing iron concentration.

The possibility that this signal corresponds to amorphous or extremely small haematite particles cannot be ruled out. Indeed, in the latter case a classic SPM behaviour is expected because the particles are well dispersed and, in addition, the interaction between α-Fe_2O_3-CuO single domains is supposed to be weaker than between the α-Fe_2O_3 ones. This same hypothesis rules out that SPM haematite can contribute to the doublet in the $x = 0.03$ sample, which does not show a co-existence of both the SPM doublet and the sextet of the blocked single domains. In addition, after annealing this sample at 750 K for 40 h, in spite of the increase in the grain size and the strain reduction achieved, no appreciable changes were observed in the population or in the hyperfine parameters of the signals. This evidences that the signal does not come from an amorphous iron phase but from the Cu(Fe)O solid solution, which has been proved to be stable under annealing in air for long periods up to 800 K [15].

4.3. Intermediate- and high-x region: the interface contribution

In the $0.30 \leqslant x \leqslant 0.95$ region, the RT Fe^{3+} doublet has an important contribution of SPM haematite. Indeed, the reduction of the thermal fluctuations leads to the blocking of the magnetic moments of these particles, as seen by the increase in the α-Fe_2O_3 population at LT (figures 3 and 4). The broad magnetic signal that appears at 30 K is different from that normally attributed to α-Fe_2O_3 small particles [28]. This might be associated either with Fe atoms at the surface of α-Fe_2O_3, in close contact with CuO particles, or to the formation of a Cu–Fe–O phase. However, the fact that this signal accounts for a significant proportion of the spectra suggests that the formation of a new phase in this high-x range should have been detected by XRD.

The complex spectra usually observed in fine-particle systems are not directly related to the presence of a new phase. As the surface-to-volume ratio increases when the particle size approaches nanoscale dimensions, a different contribution associated with the surface layer can be expected to appear in the spectra. Indeed, the atoms located near the surface have different environments in comparison to the inner ones. A nanostructured material can be thought of as consisting of building blocks (the crystallites) with a disordered region between those blocks (grain boundaries). The individual spins of the magnetic ions in the surface are supposed not to be linked to the collective behaviour of the magnetic moment of the particle in the same way as the inner ones are. The lattice distortions and the loss of magnetic neighbours due to symmetry breaking originate a weakening of exchange interactions and the presence of magnetic frustration, giving rise to spin-glass-like behaviours or canted ferromagnetic arrangements [7]. This latter assumption explains the high values of the magnetic moments and the appearance of additional Mössbauer components that have been found previously in nanocrystalline α-Fe_2O_3 [7, 29]. Van der Kraan [30] showed that surface ions of ultrafine α-Fe_2O_3 have a distributed B_{hf}, and its value is lower than that obtained for the bulk component. Furthermore, the null 2ε value reported for the surface component was assigned to the random orientation between the magnetization vector of the particle and the electric field gradient.

Due to the preparation method that we have employed our samples differ from a system of well dispersed particles. The proportion of CuO in the mixture influences the proximity of α-Fe_2O_3 particles, and thus the exchange interactions between atoms at their surfaces. In addition, the interface between α-Fe_2O_3 particles could be seen as an iron-rich Cu–Fe–O solid solution, with varying properties, relative fraction and composition, as x changes. Thus, the broad magnetic sextet that has a reduced B_{hf} value with respect to that of bulk haematite might

be related to this interface. The high relative area associated with the ferric oxide surface for the $x = 0.67$ and 0.80 samples can be explained by the presence of a wide layer where the Fe atoms have a disordered environment. This is probably originated in the damage induced by the BM and, additionally, the disorder introduced by the presence of Cu^{2+} ions with a different spin, exchange constants and oxygen co-ordination. This interface contribution is seen to decrease with x, and finally disappears for $x = 1.00$. The absence of a well distinguishable interface signal at 30 K in the ball-milled pure haematite can be understood by the partial recovery of the particle size, the absence of chemical perturbation, and the relevance of particle agglomeration. While the first factor leads to a lower surface-to-volume ratio, the second and third bring on the vanishing of a net difference between the surface and core sites. It is worth noting that the LT spectrum for $x = 0.30$ shows a significant relaxation feature and—within a static picture—a lower B_{hf}. This could be in relation to the signal originating in Fe nuclei sensing the CuO matrix, that might also be present for samples with $x > 0.10$ coexisting with both the bulk α-Fe_2O_3 and the grain boundary signals.

It is interesting to note that the $x = 0.67$ sample corresponds to the 1:1 molar ratio necessary to prepare the ferrite $CuFe_2O_4$. This compound is a Cu–Fe–O stable phase that is usually obtained by a solid-state reaction at high temperature [15]. The fact that the BM leads to a decrease in the grain sizes and then increases the contact area between the reactants favours the formation of the products at nominal room temperature. Indeed, from magnetization results, $CuFe_2O_4$ has been reported to form after prolonged BM in a 1:1 α-Fe_2O_3/CuO mixture using a high-energy planetary mill [16]. However, the authors could not identify the $CuFe_2O_4$ signal clearly either from the x-ray patterns or from the Mössbauer results. The latter showed at RT a doublet with the typical parameters of SPM iron oxides. In our sample, we observe that the doublet partially gives rise to a distributed magnetic component at LT. The $B_{hf} \approx 40$ T is far below that reported for both cubic and tetragonal $CuFe_2O_4$ [31] as well as from the $B_{hf}(4.2\ \mathrm{K})$ average values assigned to the ball-milled spinel in [16].

At RT, both $x = 0.95$ and $x = 1.00$ samples display a relaxation behaviour as well as contribution of additional magnetic components. Nevertheless, the LT spectrum for $x = 1.00$ shows that there is only one magnetic site that belongs to haematite in its WF state. In this case, as we showed in a previous work [13], the RT additional contributions were originated in magnetic interparticle interactions. The more relaxed RT spectrum seen for the $x = 0.95$ sample can be explained noting that their particle size is somewhat smaller than that of the $x = 1.00$ one according to the XRD analysis (figure 2). In addition, an increase in the mean interparticle separation due to the CuO particles would bring about a weakened interparticle interaction. Having a small magnetic moment per particle, the interaction between haematite particles would be mainly due to the exchange between atoms located at the interfaces, and thus, strongly sensitive to any variation in the interparticle distance [13].

It is worth noting that a Mössbauer signal with a $B_{hf} \approx 47$ T, with similar features to those we assign to the grain boundaries, has been reported for amorphous Fe_2O_3 [32]. In that case, the signal displays an AF order below 80 K and the magnetization is of the order of that of bulk haematite. Thus, in our case, the hypothesis that the distributed magnetic component could correspond to amorphous material cannot be ruled out.

4.4. Analysis of the magnetic measurements

The magnitude of the residual M_0 values recorded at RT and 10 K also argue against the formation of a spinel phase in large percentage (figure 6). For AF small particles, M_0 embraces the contribution of both the uncompensated moments of the sublattices and the disordered spins situated at the surface [33]. Furthermore, in the samples with high α-Fe_2O_3 content, a

contribution from the small WF moment can also be expected [33]. The higher M_0 values registered for samples $x = 0.67$ and 0.80 might be related with a major spin disorder near the surface. Moreover, the LT Mössbauer spectra of these samples show that the contribution from the broad sextet, different from the haematite one, is present in a high percentage. These samples are found to have the smallest particle sizes within the series and thus the surface contribution is expected to be important. This is in agreement with the higher fields which are needed to align the moments in the $x = 0.67$ sample at 10 K. Indeed, the fact that the initial magnetization curve remains below the remagnetization one can be explained by the presence of random frozen spins that are located at the surface [8]. At low fields and temperatures, the random surface exchange anisotropy does not allow the spins at the surface to be immediately aligned with the applied field. But as soon as the field is strong enough to force the surface spins to align with it a coherent spin rotation is possible. Thus, the sample can be demagnetized with a low H_c (table 2) and remagnetized more easily. The same behaviour has been observed for interacting α-Fe_2O_3 nanoparticles [8].

5. Conclusions

The ball milling of CuO/α-Fe_2O_3 mixtures in a vertical vibratory mill produced only nanoparticles of CuO and α-Fe_2O_3 for all concentrations. The CuO crystallites show a degree of strain higher than that of α-Fe_2O_3. The haematite grain size depends noticeably on the nominal composition, showing a minimum size for intermediate x. At low x, a solid solution of Cu(Fe)O was formed with a relaxation regime similar to that previously observed in samples obtained by mechanical and chemical methods. As x increases, the superparamagnetic haematite fraction increases and, in addition, the Mössbauer spectra at 30 K show the appearance of a broad magnetic signal that we assign to an iron-rich solid solution formed at the α-Fe_2O_3-CuO interface. In addition, the $x = 0.67$ sample demonstrates an anomalous hysteresis at low temperature that we associate with an important degree of spin disorder in the interfaces that freezes at low temperature.

Acknowledgments

Partial economic support by CONICET (PIP 4326 and PIA 7102), ANPCyT (PICT 1135 and 1277), and CICPBA, Argentina, is gratefully acknowledged. SJS and RAB are fellows of CONICET, GP and RCM are members of Carrera del Investigador Científico, CONICET. The x-ray diffraction analyses were carried out in the LANADI facilities at La Plata. RAB thanks R D Zysler for useful conversations. We are grateful to C Johnson for proofreading the manuscript. FG acknowledges CNPq for financial support.

References

[1] Campbell S J and Gleiter H 1993 *Mössbauer Spectroscopy Applied to Magnetizm and Materials Science* ed G L Long and F Grandjean (New York: Plenum) p 241
[2] Ding J, Miao W F, Pirault E, Street R and McCormick P 1998 *J. Alloys Compounds* **267** 199
[3] See, for example, Eckert J, Holzer J C, Krill C E III and Johnson W L 1993 *J. Appl. Phys.* **73** 2794
[4] Kosmac T and Courtney T H 1992 *J. Mater. Res.* **7** 1519
[5] Bonetti E, Del Bianco L, Fiorani D, Rinaldi D, Caciuffo R and Hernando A 1999 *Phys. Rev. Lett.* **83** 2829
[6] Kodama R H, Berkowitz A E, McNiff E J Jr and Foner S 1996 *Phys. Rev. Lett.* **77** 394
[7] Dimitrov D V, Hadjipanayis G C, Papaefthymiou V and Simopoulos A 1998 *J. Magn. Magn. Mater.* **188** 8
[8] Zysler R D, Fiorani D and Testa A M *J. Magn. Magn. Mater.* unpublished
[9] Del Bianco L, Hernando A, Bonetti E and Navarro E 1997 *Phys. Rev.* B **56** 8894

[10] Morish A H 1994 *Canted Antiferromagnetizm: Hematite* (Singapore: World Scientific)
[11] Forsyth J B, Brown P L and Wanklyn B M 1988 *J. Phys. C: Solid State Phys.* **21** 2917
[12] Campbell S J, Kaczmarek W A and Wang G M 1995 *NanoStruct. Mater.* **6** 735
[13] Borzi R A, Stewart S J, Punte G, Mercader R C, Vasquez-Mansilla M, Zysler R D and Cabanillas E D 1999 *J. Magn. Magn. Mater.* **205** 234
[14] Borzi R A, Stewart S J, Punte G, Mercader R C and Garcia F *J. Magn. Magn. Mater.* unpublished
[15] Stewart S J, Borzi R A, Punte G and Mercader R C 1998 *Phys. Rev.* B **57** 4983
[16] Goya G F and Rechenberg H R 1998 *J. Phys.: Condens. Matter* **10** 11 829
[17] Sakthivel A and Young R A 1991 *DBWS-9006PC* program for Rietveld analysis of x-ray powder diffraction patterns, Georgia Institute of Technology, Atlanta
[18] Krumm S 2000 *WinFit 1.2* program to fit and analyse x-ray powder diffraction lines, Institut fur Geologie, Erlangen
[19] Klug H P and Alexander L E 1974 *X-Ray Diffraction Procedures for Polycrystalline and Amorphous Materials* 2nd edn (New York: Wiley)
[20] Delhez R, de Keijser T H, Langford J I, Loüer D, Mittemeijer E J and Sonnelved E J 1993 *The Rietveld Method* ed R A Young (Oxford: Oxford University Press)
[21] Roberts W L, Campbell T J and Rapp G R Jr 1990 *Encyclopedia of Minerals* 2nd edn (New York: Van Nostrand Reinhold)
[22] Dang M Z, Rancourt D G, Dutrizac J E, Lamarche G and Provencher R 1998 *Hyperfine Interact.* **117** 271
[23] Masterov V, Nasredinov F S, Daribaeva G T, Kovelev V F, Seregin P P and Tritskaya N 1991 *Sov. Phys.–Solid State* **33** 1525
[24] Borzi R A, Stewart S J, Punte G, Mercader R C, Curutchet G A, Zysler R D and Tovar M 2000 *J. Appl. Phys.* **87** 4870
[25] Cullity B D 1972 *Introduction to Magnetic Materials* (Reading, MA: Addison-Wesley) p 197
[26] Ohyama S and Kishida H 1999 *Appl. Catal.* A **184** 239
[27] Murad E 1992 *Studies of Magnetic Properties of Fine Particles and their Relevance in Materials Science* ed J L Dormann and D Fiorani (Amsterdam: Elsevier)
[28] Kündig W, Bömmel H, Constabaris G and Lindquist R H 1966 *Phys. Rev.* **142** 327
[29] Vasquez-Mansilla M, Zysler R D, Arciprete C, Dimitrijewits M I, Saragovi C and Greneche J M 1999 *J. Magn. Magn. Mater.* **204** 29
[30] Van Der Kraan A M 1973 *Phys. Status Solidi* a **18** 215
[31] Evans B J and Hafner S S 1968 *J. Phys. Chem. Solids* **29** 1573
[32] Van Diepen A M and Popma Th J A 1976 *J. Physique Coll.* **37** C6 755
[33] Bødker F, Hansen M F, Koch C B, Lefmann K and Mørup S 2000 *Phys. Rev.* B **61** 6826